Biosensors and Bioelectronics 146 (2019) 111760

Contents lists available at ScienceDirect

Biosensors and Bioelectronics

journal homepage: http://www.elsevier.com/locate/bios

A novel optical fiber glucose biosensor based on carbon quantum dots-glucose oxidase/cellulose acetate complex sensitive film

Sha Yu, Liyun Ding *, Haitao Lin, Wei Wu, Jun Huang

National Engineering Laboratory for Fiber-optic Sensing Technology, Wuhan University of Technology, Wuhan, 430070, China

ARTICLE INFO

Keywords:
Glucose sensing
Optical fiber
Carbon quantum dots-glucose oxidase/cellulose acetate complex sensitive film
Fluorescence quenching

ABSTRACT

A novel optical fiber glucose biosensor based on fluorescent carbon quantum dots (CQDs)-glucose oxidase (GOD)/cellulose acetate (CA) complex sensitive film was fabricated, in which the dip-coating method was adopted to immobilize the CQDs-GOD/CA complex sensitive film onto the end face of the optical fiber. The surface morphology, microstructure and optical performances of the sensitive film were characterized by field emission scanning electron microscope (FESEM), atomic force microscope (AFM), Zeiss Axiovert 25 inverted microscope, Fourier transform infrared spectroscopy (FTIR), Ultraviolet–visible spectrophotometer and fluorescence spectrophotometer, respectively. The developed fiber-optic biosensor exhibits high sensitivity and repeatability for continuous online detection of low concentration glucose, allowing visualization of real-time glucose fluctuations over a period of time. The change ratios in fluorescence intensity of the biosensor are linear with glucose concentration in various ranges including micromole and nanomole levels, and the relationship between relative fluorescence intensity ratio and glucose concentration complies well with the modified Stern-Volmer equation in the range of 10–200 μmol/L with the detection limit of 6.43 μM, and in the range of 10–100 nmol/L with the detection limit of 25.79 nM, respectively.

1. Introduction

As the main energy source and the metabolic intermediate of living cells, glucose plays a vital role in organisms, and its level in human body is closely related to human health. Higher blood glucose can lead to diabetes and induce diverse serious complications, threatening human health and life safety. Therefore, the detection of glucose is significant for the prevention and treatment of diseases (Guo and Ma, 2017). Although the monitoring of blood glucose in the organism is important since blood is by far the most understood diagnostic sample, other biological fluids such as tears, saliva and sweat containing lots of biochemical analytes also provide valuable information as well as being more available than blood (Liao et al., 2015; Makaram et al., 2014). In order to monitor the information about metabolic physiological processes while detecting glucose noninvasively, it's generally possible to obtain relevant information by measuring the glucose in body fluids or metabolic fluids other than blood (Olarte et al., 2013; Yan et al., 2011). However, the diversity of biological metabolism causes certain differences in glucose level of metabolic products where the glucose content is usually much lower than that in blood (Moyer et al., 2012), as the glucose concentration in saliva of normal people is 30–80 μM (Wang et al., 2016), while that in tears is just about 2–3% of blood glucose. Also, such techniques and methods for trace glucose detection in biological fluids are still lacking and need to be exploited. In addition to clinical diagnosis, the development and optimization of detection technology for trace glucose is necessary to promote its application in other fields including environmental monitoring, biomedicine like the assessment of embryonic development and food analysis like the determination of residual sugar. Diverse glucose sensors have been developed recently including capacitive sensors (Zhang et al., 2017), electrochemical sensors (Meng et al., 2018), fluorescent sensors (Benito-Pena et al., 2016; Liu et al., 2018), optical sensors (Shehab et al., 2017). Among these sensors, electrochemical and optical ones have been widely used due to good stability and reliable measurement accuracy. However, some electrochemical glucose sensors (including the GOD-based ones and those based on noble metals and their alloys, transition metals and their oxides) are usually high-cost and susceptible to external factors such as electromagnetic field, temperature, pH value and ambient relative humidity, which greatly limits their practical applications (Su et al., 2016; Yang et al., 2016).

* Corresponding author.
E-mail address: dlyw@whut.edu.cn (L. Ding).

https://doi.org/10.1016/j.bios.2019.111760
Received 1 August 2019; Received in revised form 26 August 2019; Accepted 2 October 2019
Available online 3 October 2019

In contrast, as a kind of optical sensor, the fiber-optic sensors have attracted much attention in sensing field owing to their strong anti-interference ability, high sensitivity, fast response, remote control and strong adaptability (Li et al., 2018). The detection principles of the current fiber-optic glucose sensors are mostly based on surface plasmon resonance (SPR) (Yuan et al., 2018), localized surface plasmon resonance (LSPR) (Jiang et al., 2017), Fabry-Perot (F-P) interferometry (Khan et al., 2018), intensity modulation (Pahurkar et al., 2015), pulse width modulation (PWM) (Tang et al., 2013), phase modulation (Huang et al., 2016) and wavelength shift (Jiang et al., 2018). Nevertheless, these aforementioned sensors utilizing the intrinsic characteristics of the optical fiber have more or less drawbacks which haven't been addressed such as the complicated structure, the limitation of the optical interaction length, the mutual interference between optical signals, and difficult signal processing, tremendously restricting their detection limit and sensitivity (Yuan et al., 2017). In comparison, the fluorescence-based biosensors using fluorescence intensity or fluorescence decay as the sensing signal have been confirmed to be a prevalent optical detection technique in biosensing (Cho and Park, 2019). With the increasing maturity of fiber-optic sensing technology and the advancement of nano-material preparation, highly efficient fiber-optic glucose biosensors have been developed by immobilizing sensitive materials onto optical fibers, which can achieve accurate, fast, and real-time glucose detection. As a superior fluorescent nanomaterial, carbon quantum dots (CQDs) has become a research frontier in biosensing due to its water solubility, high photostability, low toxicity, good biocompatibility (Wang et al., 2017). Correspondingly, enzyme-based optical fiber biosensors integrating nanoparticles, immobilized enzymes, composite membranes and other technologies, present great potential in many fields especially in complex environments with narrow and limited monitoring space because of their small size, light weight, strong selectivity and high flexibility (Bidmanova et al., 2010). Still, there are few studies focus on the fluorescent detection of glucose using enzyme-based optical fiber sensors. Trettnak et al. (1988) presented a fiber-optic glucose sensor by immobilizing glucose oxidase and pH-sensitive dye in a sensing layer at the end of a fibre, where the fluorescence response of the sensor to glucose was due to the pH change of the dye. The sensor has a narrow detection limit of 0.1–2 mM with a response time in 8–12 min. Rosenzweig and Kopelman (1996) fabricated a micrometer-sized fiber-optic fluorescence biosensor, which can fast response to 1–10 mM of glucose. Scully et al. (2007) demonstrated a novel enzyme-based optical sensor for in situ continuous monitoring of glucose with a detection limit of 0.1 mM over a range up to 30 mM. Siegrist et al. (2010) reported a fluorescent hydrogel-based GRP sensor with high hypoglycemic sensitivity and precision.

Given that the micron-sized quartz optical fibers have large mode area and high light transmission efficiency, we developed a novel enzyme-based fluorescent fiber-optic glucose biosensor using the 600 μm quartz optical fiber coated with CQDs-GOD/CA sensitive film, in which the CQDs-GOD complex with enzymatic activity as the fluorescence indicator. The characteristics of the sensitive film were studied by various analysis and testing techniques. Based on the fluorescence quenching of the film on the fiber-optic probe, the typical fluorescence response curve of the sensor to glucose could be found. The proposed glucose biosensor provides a new platform for trace glucose sensing applications.

2. Materials and methods

2.1. Reagents and chemicals

L-Cysteine (BR) were obtained from Regal Co. Ltd. Citric acid monohydrate (99.5%), D-glucose (99%), cellulose acetate (99.5%), acetone (AR), ethanol (AR) were purchased from Sinopharm Chemical Reagent Co., Ltd. 1-(3-Dimethylaminopropyl)-3-ethylcarbodiimide (EDC) (AR), N-Hydroxysuccinimide (NHS) (AR) were bought from Sigma-Aldrich. Glucose oxidase (GOD) (BR) was acquired from Kaiyang Co. Ltd. Phosphate Buffered Saline (PBS) was prepared by disodium hydrogen phosphate (Na_2HPO_4) and sodium dihydrogen phosphate (NaH_2PO_4). Deionized water produced by the Hitech-K flow water purification system was used throughout the experiments.

2.2. Instruments and characterizations

Fluorescence measurements were performed on an F-4500 FL Spectrophotometer (Hitachi, Japan). Fourier transform infrared (FT-IR) spectra were obtained from a KBr window on a Nicolet6700 spectrometer. The end face topography of the fibre-optic probe was observed by a Zeiss Axiovert 25 inverted microscope. The morphological characterizations of the CQDs-GOD/CA complex sensitive film were evaluated by atomic force microscope (AFM) (Nanoscope IV, USA) and JEM-7500F field emission scanning electron microscope (FESEM) operated at 5.0 kV. The 405 nm violet diode laser (MDL–III–405-100 mW) and QE65000 spectrometer (Ocean Optics) equipped with a back-thinned CCD detector were employed to construct the optical sensing platform.

2.3. Preparation of complex sensitive film and sensor probe

The CQDs-GOD complex was prepared by the chemical cross-linking method, in which the fluorescent CQDs were synthesized by one-step microwave assisted method using L-cysteine and citric acid monohydrate as precursors. Concisely, 2 mL of the purified CQDs solution and 7.4% (v/v) of 0.1 mol/L EDC/NHS solution were mixed in PBS (pH = 6.5) and stirred slowly for 1 h at room temperature. Then 0.5 mL GOD solution (1.0 mg/mL) was added to the mixture with constant stirring at 4 °C for 2 h. The obtained solution was dialyzed (MWCO: 8 kDa) for two days in a 4 °C refrigerator to remove unreacted precursors and small molecule products.

The CQDs-GOD/CA complex sensitive film was prepared as follows: 0.108 g cellulose acetate and 3.0 mL acetone were mixed in a penicillin bottle under magnetic stirring for 2 h, followed by adding 0.3 mL CQDs-GOD complex into it and stirred at 4 °C for 6 h. The solution was then transferred into a refrigerator and stored at 4 °C until a viscous casting solution was formed. As for the preparation of sensing probe, 600 μm quartz optical fibers with high coupling efficiency and negligible fiber loss were used for our experiments. Firstly, the fibers with part of whose coating removed were cut into 10 cm length and washed by deionized water and ethanol for three times, followed by natural drying at room temperature for 15 min. Subsequently, the CQDs-GOD/CA precursor casting solution was deposited on the cleaned fiber end face by dip-coating method through a vertical coating lifting machine (the parameters of coating procedure: pulling rate was 50 mm/min, dipping rate was 20 mm/min with a dipping time of 10 s and coating time of 20 s). Finally the fiber coated with the casting solution was stored in a 4 °C refrigerator for natural drying to ensure the thorough volatilization of the acetone, allowing the formation of the CQDs-GOD/CA complex sensitive film and the firm immobilization onto the fiber end face. Moreover, the CQDs-GOD/CA complex sensitive film coated onto a 10 mm × 10 mm × 0.43 mm silicon polished wafer by the same dip-coating method was also obtained and used for a series of characterizations.

2.4. Construction of optical platform for glucose detection

The schematic illustration of the optical experimental platform used to verify the performance of the fiber-optic glucose biosensor is shown in Fig. 1. The high-stable incident laser provided by the 405 nm violet diode laser is divided into two parts by the dichroic mirror after passing through the attenuator. One-part light with the long-wavelength is transmitted through the spectroscope and monitored by the optical power meter. The other part light of the short-wavelength is reflected by the spectroscope for sensing purpose. After focusing with a 4 × objective

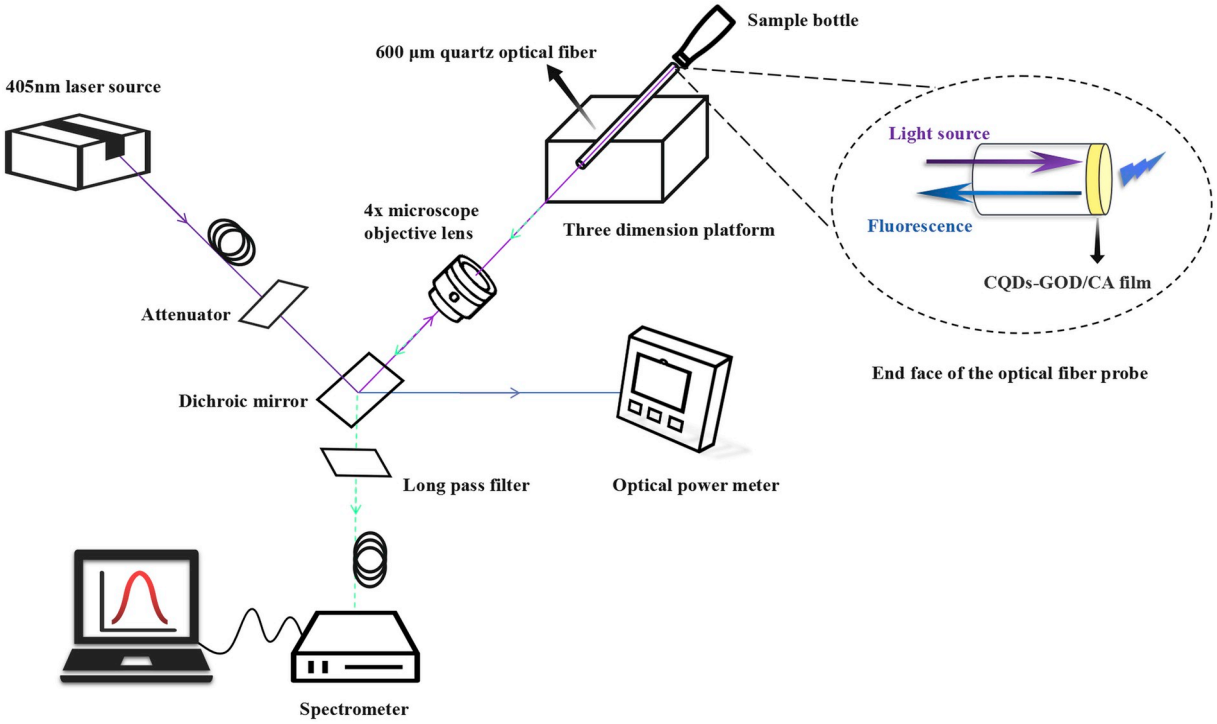

Fig. 1. The schematic diagram of the optical fiber sensor platform.

lens (numerical aperture 0.10), the reflected light is coupled into the optical fiber core by adjusting the three-dimensional platform, and then propagates along the core to the other end of the fiber, thus exciting the sensitive film on the end face to generate fluorescence. The induced fluorescence signal is transmitted back along the fiber then successively passes through the objective lens, dichroscope, the high-pass filter and eventually received and processed by the spectrometer and the computer.

2.5. Glucose detection by the optical fiber biosensor

Some researches have reported that CQDs-based materials are excellent detectors for H_2O_2 since their fluorescence can be effectively quenched by H_2O_2 due to the charge transfer (CT) or electron transfer (ET) mechanism (Chu et al., 2016; Qian et al., 2014; Shan et al., 2014; Sadhukhan et al., 2014; Shen et al., 2017). In this work, the principle of optical fiber biosensor for glucose detection is based on the fluorescence quenching of the CQDs-GOD/CA complex sensitive film induced by the enzymatic conversion of glucose to H_2O_2. Exactly, when the sensor probe was dipped into the tested glucose solution, the glucose would penetrate into the sensitive film and participate in the enzymatic reaction with the embedded indicator CQDs-GOD to generate H_2O_2, thus decreasing the fluorescence intensity of the sensor probe. Since there are dependent relationships between the glucose concentration and the relative fluorescence intensity ratio, the quantitative analysis of glucose can be achieved through the fluorescence response of the sensor to glucose. In the glucose measurement, the as-prepared sensor probe was firstly fixed on a three-dimensional platform (Fig. 1) and then dipped into a 1.5 mL glass bottle containing glucose solution, the generated fluorescence signal was collected and analyzed by the spectrometer. Thereby, a series of standard glucose solutions with different concentrations were then measured to obtain the calibration curves of the glucose biosensor.

3. Results and discussion

3.1. Optical properties of the CQDs-GOD/CA complex sensitive film

The fluorescence emission spectra of the CQDs-GOD/CA complex sensitive film and the CQDs-GOD complex are shown in Fig. 2. The inset are the photographs of the sensitive film under daylight (left) and a 365 nm UV lamp (right). It can be seen that the CQDs-GOD/CA complex sensitive film emits blue fluorescence at 448 nm under the optimal excitation wavelength of 345 nm. In addition to excellent fluorescence emission property, the sensitive film also exhibits the anti-photobleaching performance (Fig. S10).

Besides, we found that the fluorescence intensity of the CQDs-GOD/

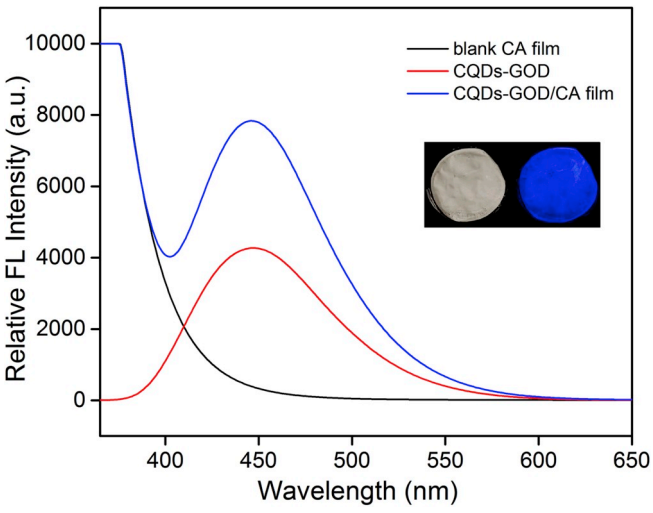

Fig. 2. The fluorescence emission spectra of the CQDs-GOD/CA complex sensitive film, the CQDs-GOD complex and the CA film, respectively. Inset: photographs of the CQDs-GOD/CA complex sensitive film under daylight (left) and 365 nm ultraviolet lamp (right).

CA complex sensitive film was enhanced significantly compared with that of the CQDs-GOD complex. In order to explore the reason for the enhancement of fluorescence after film formation, the structure and composition of the CQDs-GOD complex and the CQDs-GOD/CA film were investigated by FT-IR (Fig. S1). The absorption peak at 1521 cm^{-1} was attributed to the stretching vibration of C–N–H, indicating the existence of secondary amine groups (–NH–) in the CQDs-GOD complex. Peaks at around 1720 cm^{-1} were determined as C═O stretching vibration on the carboxyl groups (-COOH). The vibration absorption peak at 1640 cm^{-1} was corresponded to primary amide groups (–CO–NH-). The sharp double peaks at 1430 and 1360 cm^{-1} were associated with the C–N stretching vibration of amide III band. Peaks appeared at 1240 cm^{-1} were attributed to C–O stretching vibration. Peaks at 1050 cm^{-1} were identified as C–OH vibration absorption. It's evident that the C═O peak intensity of carboxyl groups was decreased while that of the primary amide (1640 cm^{-1}) was significantly increased. The secondary amine peak at 1521 cm^{-1} was disappeared and replaced by a primary amine double peak at around 1400 cm^{-1}. These results indicate that a large amount of secondary amides (–CO–NH–CO–) in CQDs-GOD complex were converted into primary amides (–CO–NH-), and the C═O bonds were reduced to C–O bonds during the film formation process, leading to the surface passivation of the CQDs-GOD complex, thus enhancing the fluorescence intensity of CQDs-GOD/CA complex sensitive film. As many researches focusing on the mechanism of CQDs luminescence have demonstrated that the surface passivation of the nanoparticles would great increase its fluorescence intensity, since the photoluminescence from CQDs may be ascribed to the surface energy traps that get emissive upon stabilization due to the surface passivation (Pan et al., 2017; Sun et al., 2006). Therefore, the passivation of CQDs-GOD complex surface is equivalent to the surface passivation of CQDs with amino groups, resulting in the enhancement of the fluorescence.

3.2. Surface topography of the CQDs-GOD/CA complex sensitive film

The end face topography of the optical fiber probe was observed by an inverted microscope, and the photomicrographs of the fiber end face without and with the CQDs-GOD/CA complex sensitive film are shown in Fig. S2. It is obvious that the fiber end face coated with sensitive film is rougher than that of uncoated one, indicating that the sensitive film is uneven and has a certain roughness and thickness. This observation and more specific details about the sensitive film are supported by subsequent AFM (Fig. 3) and FESEM images (Fig. 4). Fig. 3 shows that the film coated onto the fiber end face is rough with a thickness of about 300 nm. And the film has a porous structure with the average hole diameter of

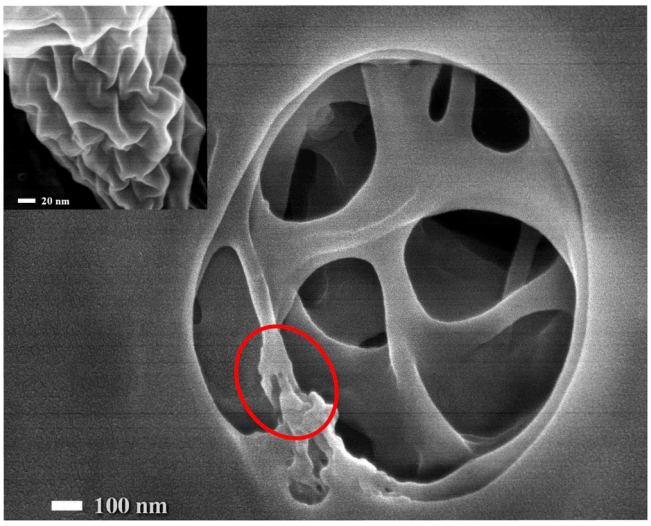

Fig. 4. FESEM images of the CQDs-GOD/CA complex sensitive film. Inset: the partial enlarged detail of the marked area.

0.5 μm, which provides sufficient permeability to ensure the adequate diffusion of glucose within the prescribed response time.

Fig. S6 (the SEM image of lower magnification to show the larger area of the film) and Fig. 4 illustrate that there are many micron-sized holes in the sensitive film, which is conducive to the penetration of glucose into the film to react with the fluorescent indicator CQDs-GOD complex. The inset in Fig. 4 reveals that the film surface is uneven and has many wrinkles, which enlarges the specific surface area and allows more fluorescent indicators CQDs-GOD attache to the film, thus enhancing the fluorescence performance of the sensitive film and improving the sensitivity of the sensor probe to glucose.

Given that the addition of the fluorescent indicator CQDs-GOD during the film preparation process will lead to an increase in the total amount of the precursor solution, thereby affecting the film formation. We investigated the effect of CQDs-GOD dosage (i.e. 0.2 mL, 0.3 mL, 0.4 mL) on the synthesis and properties of the sensitive film. As shown in Fig. S7, larger addition of the CQDs-GOD can improve the fluorescence property of the film, while excessive addition will bring about thinner and more transparent film morphology, not conducive to the formation and deposition of the film on the fiber end. These results were also well supported by the SEM images (Fig. S8). It can be seen that less CQDs-GOD dosage (0.2 mL, Fig. S8(a)) causes smaller pore structure

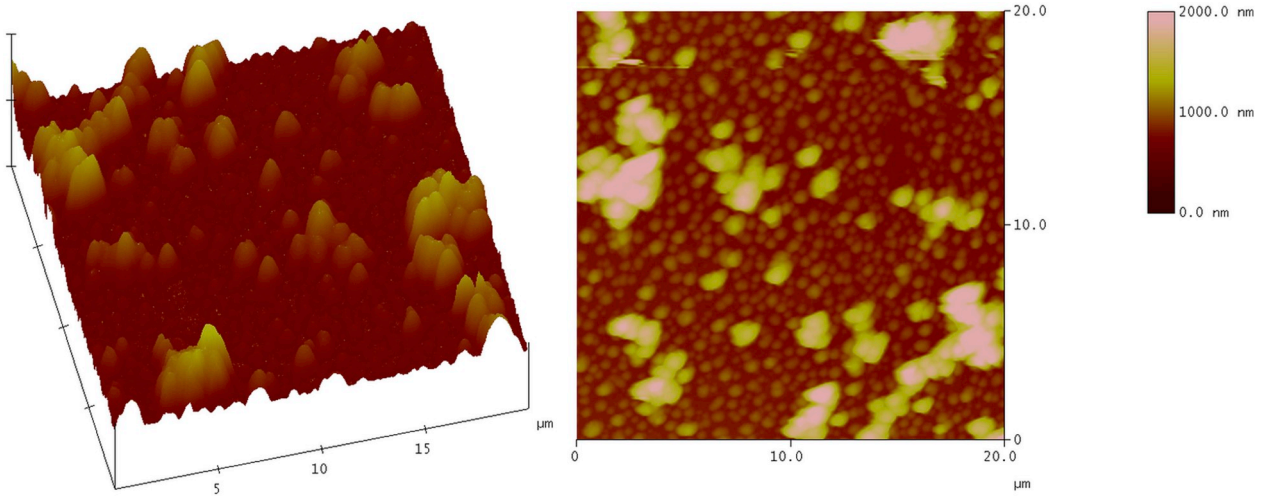

Fig. 3. AFM images of the CQDs-GOD/CA complex sensitive film.

of the CQDs-GOD/CA film, which is unfavorable for the permeation of the tested glucose. While larger dosage (0.4 mL, Fig. S8(c)) may induce bigger hole in the film, destroying its uniform structure, compared with that of 0.3 mL CQDs-GOD (Fig. S8(b)). Therefore, 0.3 mL CQDs-GOD complex was regarded as the more suitable dosage and was used during the preparation of sensitive film.

3.3. Typical fluorescence response of the optical fiber sensor to glucose

A series of standard glucose solutions with various concentrations ranging from 10 to 200 μmol/L were measured using the proposed fiber-optic biosensor (Fig. 5(a)). It can be seen that the fluorescence intensity decreased as the glucose concentration increased, which was due to the fact that more glucose penetrated into the film and participated in the enzymatic reaction to produce an increasing amount of H_2O_2. The corresponding real-time fluorescence responses of the fiber sensor to glucose solution were tested and the sequence chart was shown in Fig. 5 (b). It can be observed that the fluorescence intensity decreased sharply within 1 s and then tended to stable within 2 min as the probe was dipped into the tested solution. Here, the big drift in fluorescence signal could be attributed to the decreased refractive index difference between the optical fiber core and its surrounding medium (from quartz-air to quartz-water), since the decreased refractive index difference leads to the decreased numerical aperture (NA) of the optical fiber, allowing limited fluorescence signal to be collected and coupled back to the guided mode (Ding et al., 2018). The gradual slight decrease of the fluorescence intensity before it totally reached to the steady state was ascribed to the advancement of enzymatic reaction process. While the probe was removed from the glucose solution, the fluorescence signal recovered to a certain extent and then started to remain steady, which was consistent with the results in Fig. 5(a).

We also conducted control experiments by successively measuring a group of blank solutions (ultra-pure water) or glucose solutions (Fig. S9). In Fig. S9(a), when the probe was taken out of the water after the first immersion, the fluorescence signal intensity restored to a certain level (level A) (the incomplete recovery is due to the probe being not completely dry and still in a slightly wet state). While the probe was again dipped into water and then removed, the fluorescence intensity gradually restored and reached to level B (basically parallel to level A), which was quite different from the glucose detection results (Fig. S9(b)). The fluorescence intensity of the probe was marked as level C after the first water calibration. But when one glucose concentration measurement was completed, the fluorescence signal was not fully restored to initial level C and only reached to level D. That is, there was a certain difference in the fluorescence intensity before and after one concentration detection ($\Delta I = I_0 - I$, the difference of level C and D) because of the fluorescence quenching effect of the CQDs-GOD/CA complex sensitive film by glucose. The results in Fig. S9 demonstrated that the change of

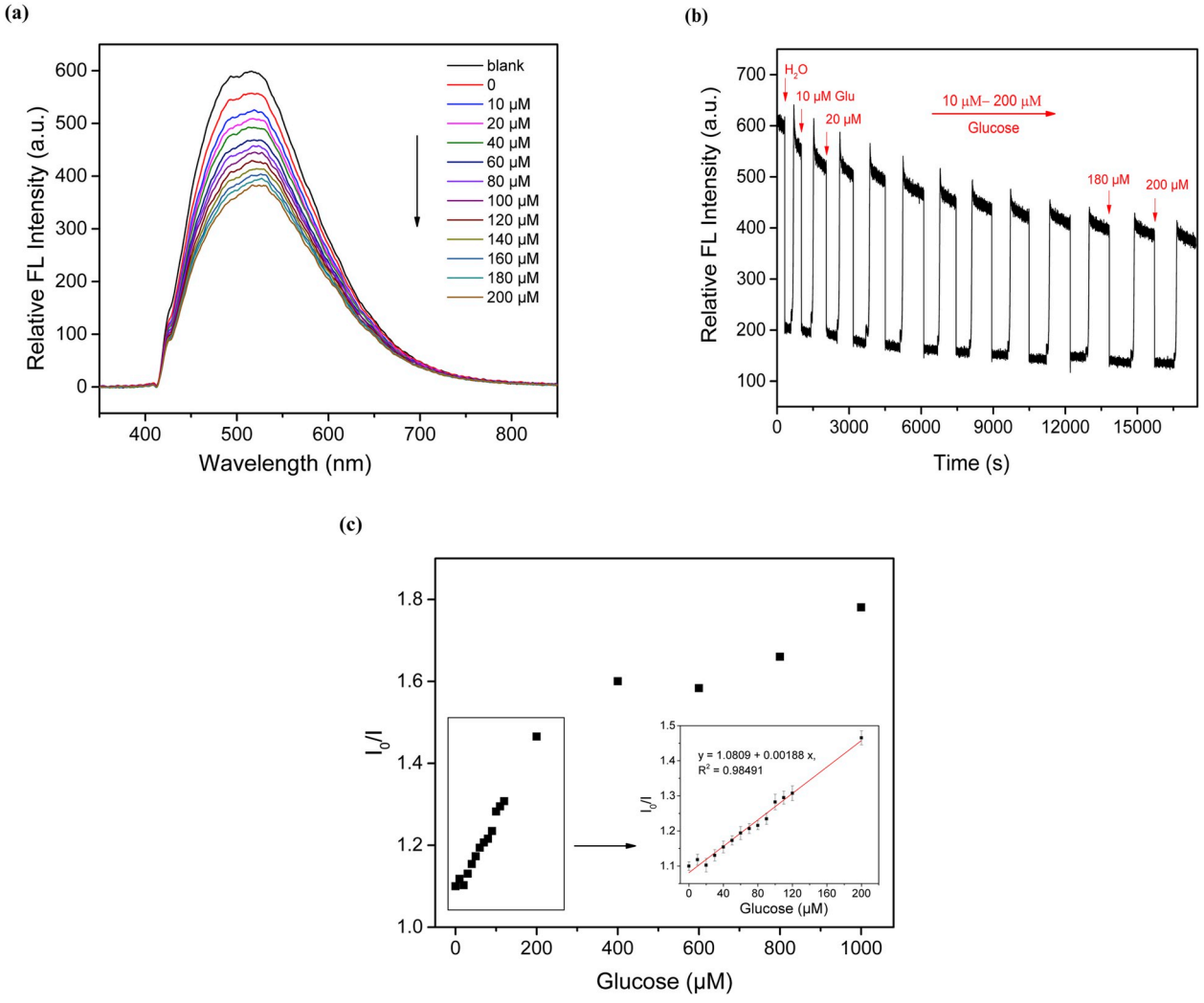

Fig. 5. The fluorescence spectra of the optical fiber sensor in the presence of glucose solution with different concentrations ranging from 10 to 200 μM (a). The glucose detection time sequence diagram (b). The calibration curve of the optical fiber sensor for the determination of glucose (c).

signal in pure water has no influence on the glucose detection.

Since the sensing mechanism of the glucose detection is based on the fluorescence quenching, the recorded data of fluorescence intensity change could be analyzed by the modified Stern-Volmer equation (Gan et al., 2012):

$$I_0 / I = K_{sv}[Glucose] + C \quad (1)$$

where I_0 and I are the fluorescence intensities of the fiber-optic sensor in the absence and presence of glucose, K_{sv} is the Stern-Volmer quenching constant, [*Glucose*] is the concentration of glucose. The fluorescence intensity ratio I_0/I exhibited dependant relationship with glucose concentration in the range of 10–200 μM as depicted in Fig. 5(c), where the calibration test results were described by the equation of $I_0/I = 0.00188$ [*Glucose*]+1.0809 ($R^2 = 0.98491$) with a detection limit of 6.43 μM (S/N = 3).

Although sensors for detecting micromolar concentrations of glucose have been reported (Jiang et al., 2017; Khan et al., 2018), there are still few studies on the trace detection of glucose. Hence we further used the prepared fiber-optic sensor to perform glucose measurements at nanomolar level in the range of 10–100 nM (Fig. S3). The calibration curve (Fig. S3(a)) is described by the formula of $I_0/I = 0.00107$ [*Glucose*]+1.04315 ($R^2 = 0.95745$) with the limit of detection estimated as 25.79 nM (S/N = 3), indicating the as-developed fiber sensor provides certain reliability and feasibility in trace glucose detection. The real-time fluorescence response of the sensor to glucose was then tested and the homologous sequence diagram was obtained in Fig. S3(b), which is similar to Fig. 5(b). Meanwhile, both the slope of the calibration curve and the correlation coefficient in Fig. 5(c) are bigger than that in Fig. S3(b), demonstrating the fiber-optic sensor shows higher sensitivity and accuracy for detecting high glucose concentrations (i.e. μM) than detecting lower ones (i.e. nM).

Additionally, a comparison of performance of typical reported fiber-optic glucose sensors and electrochemical glucose sensors are summarized in Table S1, in which the performance parameters include sensing principle/material, detection range, detection limit, sensitivity and response time toward glucose. Compared to the reported electrochemical sensors, the proposed optical fiber glucose biosensor exhibits low detection limit and wider dynamic detection ranges. While it represents high sensitivity and rapid response to glucose as compared with other fiber-optic sensors. Overall, the developed optical fiber glucose biosensor shows satisfactory integrative performances and certain advantages in trace glucose detection.

3.4. The comprehensive performance of the optical fiber glucose biosensor

In addition, we also investigated the specificity of the optical fiber sensor for glucose vs various typical guest molecules such as sucrose, fructose, lactose, glycine, L-cysteine, alanine, ascorbic acid, uric acid, and some common ions like Na^+, Cl^-, SO_4^{2-}, K^+, Ca^{2+}, Mg^{2+}, Fe^{2+}, Fe^{3+}, Cu^{2+} as shown in Fig. 6, where the interferents were all at high concentration of 1.0 mM and the glucose concentration was 100 μM, $\Delta I/I$ refers to the fluorescence quenching degree, ΔI *is* the difference between the fluorescence intensity in the absence and presence of the analyte ($\Delta I = I_0$-I). Compared with the glucose detection results, these substances have insignificant influence on the fluorescence intensity of the sensing system, as the fluorescence intensity change ratios of the sensor toward interferents were much lower ($\Delta I/I < 0.075$) than that toward glucose ($\Delta I/I = 0.269$), indicating that this fiber-optic glucose biosensor has relatively high selectivity.

The anti-interference capability is also an important indicator of sensor performance, since it is reflected in the proximity of the detected glucose concentration to the actual glucose concentration in the tested system which contains glucose and other complex interfering substances. Here, the interference rate (I.R.) was introduced to describe the anti-interference capability of the proposed biosensor. Generally, the

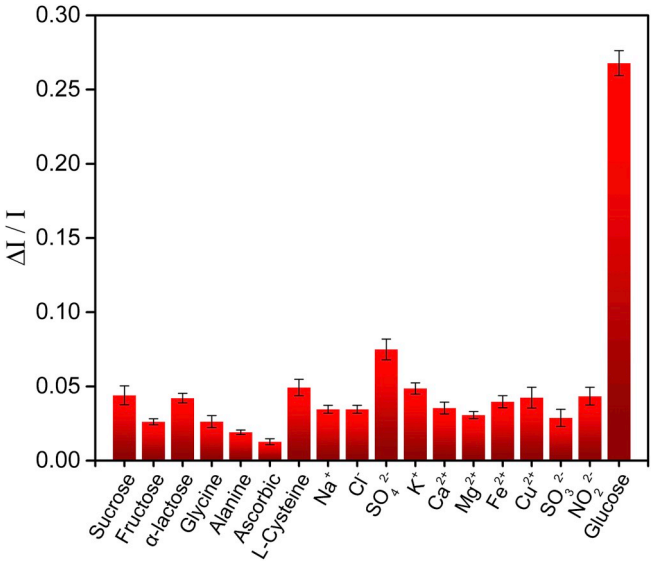

Fig. 6. The effect of different interferents on the fluorescence of the optical fiber sensor. ΔI refers to the difference between I_0 and I.

smaller interference rate (I.R) in the interference test means the stronger anti-interference ability of the sensor in detecting glucose. Considering the diversity and complexity of the actual detection environment, we established different interference systems by introducing a variety of common interfering substances (including sugars, amino acids and different ions) which are similar to the composition of human body fluids. The interference test was then conducted to study the anti-interference performance of the proposed biosensor (Fig. S4). The interference rate (I.R.) is calculated by the following formula:

$$I.R. = (C - C_0)/C_0 * 100\% \quad (2)$$

where C represents the glucose concentration detected by the constructed biosensor, C_0 is the actual substrate glucose concentration (50 μM). It can be seen that most of the interfering substances have little influence on the sensor during the glucose detection, which manifests the fiber-optic glucose biosensor has good anti-interference capability.

Furthermore, in order to evaluate the stability and repeatability of the biosensor for glucose detection, we used a separate optical fiber sensor which had been stored at 4 °C for one month to continuously detect the same specific glucose concentration (50 μM) for three times. The obtained time sequence diagrams of three independent detections are basically identical (Fig. S5), demonstrating the sensor possesses desirable stability and reproducibility with the relative standard deviation RSD of 2.97% (n = 3). Besides, the recovery test was also conducted using human serum (HS) as the practical samples to verify the performance of the proposed biosensor. All the tests were performed in triplicate measurements by adding different concentrations of glucose into HS. Here recovery (%) is the ratio of the found glucose concentration to the added glucose concentration in practical samples. The results in Table S2 suggest that the as-prepared fiber-optic biosensor is effective for the detection of real samples.

4. Conclusions

Integrating the advantages of carbon quantum dots, glucose oxidase, cellulose acetate film and large-core quartz optical fibers, we prepared a CQDs-GOD/CA complex sensitive film with both enzymatic activity and fluorescent properties, and fabricated a novel fiber-optic fluorescent biosensor for glucose by coating the sensitive film onto the end face of the optical fiber. Based on the fluorescence quenching of the sensitive film, the biosensor manifests typical rapid fluorescence response to

glucose, exhibiting not only comparable performances with previously reported sensors but also high selectivity, repeatability and anti-interference ability for continuous real-time detection of low concentration glucose. It is believed that the fabrication of this biosensor could promote the development of fluorescent fiber-optic glucose sensor. More importantly, the proposed biosensor provides a promising application for glucose trace detection in some complex environments including environmental monitoring, food analysis and biomedical fields.

Despite that the feasibility and reliability of the proposed biosensor for trace glucose detection have been verified since it indeed shows fluorescence response toward glucose at nanomolar level, the exactness, sensitivity and detection limit of the sensor in the quantitative analysis of trace glucose are still restricted due to the small difference of fluorescence signal change. Therefore, in the future work, we will devote to the performance optimization of the optical fiber sensor through the improvement of signal collection system and the preparation of the sensing probe.

Declaration of competing interest

The authors declare that they have no known competing financial interests or personal relationships that could have appeared to influence the work reported in this paper.

CRediT authorship contribution statement

Sha Yu: Methodology, Validation, Formal analysis, Investigation, Data curation, Writing - original draft, Writing - review & editing. **Liyun Ding:** Conceptualization, Resources, Writing - review & editing, Supervision. **Haitao Lin:** Methodology, Data curation. **Wei Wu:** Investigation, Data curation. **Jun Huang:** Resources, Supervision.

Acknowledgements

This work was supported by Financial Support from the National Natural Science Foundation of China (NO. 51878524, NO. 61575150).

Appendix A. Supplementary data

Supplementary data to this article can be found online at https://doi.org/10.1016/j.bios.2019.111760.

References

Benito-Pena, E., Valdes, M.G., Glahn-Martinez, B., Moreno-Bondi, M.C., 2016. Anal. Chim. Acta 943, 17–40.
Bidmanova, S., Chaloupkova, R., Damborsky, J., Prokop, Z., 2010. Anal. Bioanal. Chem. 398, 1891–1898.
Cho, M., Park, S., 2019. Sens. Actuators, B 719–729.
Chu, C., Hsieh, M., Su, Z., 2016. Hydrogen Peroxide Sensing Based on Carbon Quantum Dots. EDP Sciences, Hong Kong.
Ding, L., Ruan, Y., Li, T., Huang, J., Warren-Smith, S.C., Ebendorff-Heidepriem, H., Monro, T.M., 2018. Sens. Actuators, B 273, 9–17.
Gan, T., Zhang, Y., Zhao, N., Xiao, X., Yin, G., Yu, S., Wang, H., Duan, J., Shi, C., Liu, W., 2012. Spectrochim. Acta, Part A 99, 62–68.
Guo, J., Ma, X., 2017. Biosens. Bioelectron. 94, 415–419.
Huang, J., Li, M., Zhang, P., Zhang, P., Ding, L., 2016. Sens. Actuators, B 237, 24–29.
Jiang, S., Li, Z., Zhang, C., Gao, S., Li, Z., Qiu, H., Li, C., Yang, C., Liu, M., Liu, Y., 2017. J. Phys. D Appl. Phys. 50.
Jiang, B., Zhou, K., Wang, C., Sun, Q., Yin, G., Tai, Z., Wilson, K., Zhao, J., Zhang, L., 2018. Sens. Actuators, B 254, 1033–1039.
Khan, M.R.R., Watekar, A.V., Kang, S., 2018. IEEE Sens. J. 18, 1528–1538.
Li, Y., Ma, H., Gan, L., Liu, Q., Yan, Z., Liu, D., Sun, Q., 2018. Sens. Actuators, B 255, 3004–3010.
Liao, C., Mak, C., Zhang, M., Chan, H.L.W., Yan, F., 2015. Adv. Mater. 27, 676–681.
Liu, W., Ding, F., Wang, Y., Mao, L., Liang, R., Zou, P., Wang, X., Zhao, Q., Rao, H., 2018. Sens. Actuators, B 265, 310–317.
Makaram, P., Owens, D., Aceros, J., 2014. Diagnostics 4, 27–46.
Meng, W., Wen, Y., Dai, L., He, Z., Wang, L., 2018. Sens. Actuators, B 260, 852–860.
Moyer, J., Wilson, D., Finkelshtein, I., Wong, B., Potts, R., 2012. Diabetes Technol. Ther. 14, 398–402.
Olarte, O., Chilo, J., Pelegri-Sebastia, J., Barbe, K., Van Moer, W., 2013. Glucose Detection in Human Sweat Using an Electronic Nose. Institute of Electrical and Electronics Engineers Inc., Osaka, Japan, pp. 1462–1465.
Pahurkar, V.G., Tamgadge, Y.S., Gambhire, A.B., Muley, G.G., 2015. Measurement 61, 9–15.
Pan, J., Zheng, Z., Yang, J., Wu, Y., Lu, F., Chen, Y., Gao, W., 2017. Talanta 166, 1–7.
Qian, Z., Shan, X., Chai, L., Ma, J., Chen, J., Feng, H., 2014. ACS Appl. Mater. Interfaces 6, 6797–6805.
Rosenzweig, Z., Kopelman, R., 1996. Anal. Chem. 68, 1408–1413.
Sadhukhan, M., Bhowmik, T., Kundu, M.K., Barman, S., 2014. RSC Adv. 4, 4998–5005.
Scully, P.J., Betancor, L., Bolyo, J., Dzyadevych, S., Guisan, J.M., Fernandez-Lafuente, R., Jaffrezic-Renault, N., Kuncova, G., Matejec, V., O'Kennedy, B., Podrazky, O., Rose, K., Sasek, L., Young, J.S., 2007. Meas. Sci. Technol. 18, 3177–3186.
Shan, X., Chai, L., Ma, J., Qian, Z., Chen, J., Feng, H., 2014. Analyst 139, 2322–2325.
Shehab, M., Ebrahim, S., Soliman, M., 2017. J. Lumin. 184, 110–116.
Shen, C., Su, L., Zang, J., Li, X., Lou, Q., Shan, C., 2017. Nanoscale Res. Lett. 12.
Siegrist, J., Kazarian, T., Ensor, C., Joel, S., Madou, M., Wang, P., Daunert, S., 2010. Sens. Actuators, B 149, 51–58.
Su, Y., Luo, B., Zhang, J.Z., 2016. Anal. Chem. 88, 1617–1624.
Sun, Y., Zhou, B., Lin, Y., Wang, W., Fernando, K.A.S., Pathak, P., Meziani, M.J., Harruff, B.A., Wang, X., Wang, H., Luo, P.G., Yang, H., Kose, M.E., Chen, B., Veca, L. M., Xie, S., 2006. J. Am. Chem. Soc. 128, 7756–7757.
Tang, J., Wang, M., Chen, M., Jang, L., 2013. Glucose Detection Using an Electro-Optical Fluidic Device Based on Pulse Width Modulation. IEEE Computer Society, Wellington, New zealand, pp. 325–329.
Trettnak, W., Leiner, M.J.P., Wolfbeis, O.S., 1988. Biosensors 4, 15–26.
Wang, J., Xu, L., Lu, Y., Sheng, K., Liu, W., Chen, C., Li, Y., Dong, B., Song, H., 2016. Anal. Chem. 88, 12346–12353.
Wang, R., Lu, K., Tang, Z., Xu, Y., 2017. J. Mater. Chem. 5, 3717–3734.
Yan, Q., Peng, B., Su, G., Cohan, B.E., Major, T.C., Meyerhoff, M.E., 2011. Anal. Chem. 83, 8341–8346.
Yang, X., Yuan, Y., Dai, Z., Liu, F., Huang, J., 2016. Sens. Actuators, B 237, 150–158.
Yuan, Y., Yang, X., Gong, D., Liu, F., Hu, W., Cai, W., Huang, J., Yang, M., 2017. Opt. Express 25, 3884–3898.
Yuan, H., Ji, W., Chu, S., Qian, S., Wang, F., Masson, J., Han, X., Peng, W., 2018. Biosens. Bioelectron. 117, 637–643.
Zhang, Y., Ma, R., Zhen, X.V., Kudva, Y.C., Bühlmann, P., Koester, S.J., 2017. ACS Appl. Mater. Interfaces 9, 38863–38869.